Adaptive wavelet collocation method for PDE's on the sphere

Mani Mehra

Department of Mathematics and Statistics

McMaster University

Collaborators

- Nicholas Kevlahan (McMaster University)

Why general manifolds?

(e.g. Sphere)

- Application of adaptive wavelet collocation method (AWCM) to the problems of geodesy, climatology, meteorology (Representative examples include forecasting the moisture and cloud water fields in numerical weather prediction).
- Many PDE's arise from mean curvature flow, surface diffusion flow and Willmore flow on the sphere.

Why general manifolds?

(e.g. Sphere)

- Application of adaptive wavelet collocation method (AWCM) to the problems of geodesy, climatology, meteorology (Representative examples include forecasting the moisture and cloud water fields in numerical weather prediction).
- Many PDE's arise from mean curvature flow, surface diffusion flow and Willmore flow on the sphere.

Why general manifolds?

(e.g. Sphere)

- Application of adaptive wavelet collocation method (AWCM) to the problems of geodesy, climatology, meteorology (Representative examples include forecasting the moisture and cloud water fields in numerical weather prediction).
- Many PDE's arise from mean curvature flow, surface diffusion flow and Willmore flow on the sphere.

Why general manifolds?

(e.g. Sphere)

- Application of adaptive wavelet collocation method (AWCM) to the problems of geodesy, climatology, meteorology (Representative examples include forecasting the moisture and cloud water fields in numerical weather prediction).
- Many PDE's arise from mean curvature flow, surface diffusion flow and Willmore flow on the sphere.

Why wavelets?

- High rate of data compression.
- Fast $O(\mathcal{N})$ transform.
- Dynamic grid adaption to the local irregularities of the solution.
  (This situation arises e.g. in the tracking of storms or fronts for the simulation of global atmospheric dynamics).
- Easy to control wavelet properties (e.g. smoothness, boundary condition,better accuracy near sharp gradients).

Why wavelets?

- High rate of data compression.
- Fast $O(\mathcal{N})$ transform.
- Dynamic grid adaption to the local irregularities of the solution.
  (This situation arises e.g. in the tracking of storms or fronts for the simulation of global atmospheric dynamics).
- Easy to control wavelet properties (e.g. smoothness, boundary condition,better accuracy near sharp gradients).

Why wavelets?

- High rate of data compression.
- Fast $O(\mathcal{N})$ transform.
- Dynamic grid adaption to the local irregularities of the solution.
  (This situation arises e.g. in the tracking of storms or fronts for the simulation of global atmospheric dynamics).
- Easy to control wavelet properties (e.g. smoothness, boundary condition,better accuracy near sharp gradients).

Why wavelets?

- High rate of data compression.
- Fast $O(\mathcal{N})$ transform.
- Dynamic grid adaption to the local irregularities of the solution.
(This situation arises e.g. in the tracking of storms or fronts for the simulation of global atmospheric dynamics).
- Easy to control wavelet properties (e.g. smoothness, boundary condition,better accuracy near sharp gradients).

Why wavelets?

- High rate of data compression.
- Fast $O(\mathcal{N})$ transform.
- Dynamic grid adaption to the local irregularities of the solution.
  (This situation arises e.g. in the tracking of storms or fronts for the simulation of global atmospheric dynamics).
- Easy to control wavelet properties (e.g. smoothness, boundary condition,better accuracy near sharp gradients).

Why wavelets on manifolds?

(e.g. spherical wavelets)

- Spherical triangular grids (quasi uniform triangulations) avoid the pole problem.
  Conventional grids
  - Uniform longitude-latitude grid.
  - Another solution is to avoid the introduction of the 'metric term' which are unbounded near the poles.
- To solve PDE's efficiently using adaptivity on general manifold by wavelet methods.
- Past application of wavelets to turbulence have been mainly restricted to flat geometries which severely limiting for geophysical applications.

Why wavelets on manifolds?

(e.g. spherical wavelets)

- Spherical triangular grids (quasi uniform triangulations) avoid the pole problem.

  Conventional grids

  - Uniform longitude-latitude grid.
  - Another solution is to avoid the introduction of the 'metric term' which are unbounded near the poles.
- To solve PDE's efficiently using adaptivity on general manifold by wavelet methods.
- Past application of wavelets to turbulence have been mainly restricted to flat geometries which severely limiting for geophysical applications.

Why wavelets on manifolds?

(e.g. spherical wavelets)

- Spherical triangular grids (quasi uniform triangulations) avoid the pole problem.
  Conventional grids
  - Uniform longitude-latitude grid.
  - Another solution is to avoid the introduction of the 'metric term' which are unbounded near the poles.
- To solve PDE's efficiently using adaptivity on general manifold by wavelet methods.
- Past application of wavelets to turbulence have been mainly restricted to flat geometries which severely limiting for geophysical applications.

Why wavelets on manifolds?

(e.g. spherical wavelets)

- Spherical triangular grids (quasi uniform triangulations) avoid the pole problem.
  Conventional grids
  - Uniform longitude-latitude grid.
  - Another solution is to avoid the introduction of the 'metric term' which are unbounded near the poles.
- To solve PDE's efficiently using adaptivity on general manifold by wavelet methods.
- Past application of wavelets to turbulence have been mainly restricted to flat geometries which severely limiting for geophysical applications.

Why wavelets on manifolds?

(e.g. spherical wavelets)

- Spherical triangular grids (quasi uniform triangulations) avoid the pole problem.
  Conventional grids
  - Uniform longitude-latitude grid.
  - Another solution is to avoid the introduction of the 'metric term' which are unbounded near the poles.
- To solve PDE's efficiently using adaptivity on general manifold by wavelet methods.
- Past application of wavelets to turbulence have been mainly restricted to flat geometries which severely limiting for geophysical applications.

Why wavelets on manifolds?

(e.g. spherical wavelets)

- Spherical triangular grids (quasi uniform triangulations) avoid the pole problem.
  Conventional grids
  - Uniform longitude-latitude grid.
  - Another solution is to avoid the introduction of the 'metric term' which are unbounded near the poles.
- To solve PDE's efficiently using adaptivity on general manifold by wavelet methods.
- Past application of wavelets to turbulence have been mainly restricted to flat geometries which severely limiting for geophysical applications.

Wavelet multiresolution analysis of $L_2(S)$

Definition

MRA is characterized by the following axioms

- $V^j \subset V^{j+1}$ (subspaces are nested).
- $\overline{\bigcup_{j=-\infty}^{j=\infty} V_j} = L_2(S)$.
- Each V^j has a Riesz basis of scaling function $\{\phi_k^j | k \in \mathcal{K}^j\}$.

Define $W_j = \{\psi_k^j(\textit{wavelets}) | k \in \mathcal{M}^j\}$ to be the complement of V_j in V_{j+1}, where $V_{j+1} = V_j + W_j$.

Wavelet multiresolution analysis of $L_2(S)$

Definition

MRA is characterized by the following axioms

- $V^j \subset V^{j+1}$ (subspaces are nested).
- $\overline{\bigcup_{j=-\infty}^{j=\infty} V_j} = L_2(S)$.
- Each V^j has a Riesz basis of scaling function $\{\phi_k^j | k \in \mathcal{K}^j\}$.

Define $W_j = \{\psi_k^j(\textit{wavelets}) | k \in \mathcal{M}^j\}$ to be the complement of V_j in V_{j+1}, where $V_{j+1} = V_j + W_j$.

Wavelet multiresolution analysis of $L_2(S)$

Definition

MRA is characterized by the following axioms

- $V^j \subset V^{j+1}$ (subspaces are nested).
- $\overline{\bigcup_{j=-\infty}^{j=\infty} V_j} = L_2(S)$.
- Each V^j has a Riesz basis of scaling function $\{\phi_k^j | k \in \mathcal{K}^j\}$.

Define $W_j = \{\psi_k^j(\textit{wavelets}) | k \in \mathcal{M}^j\}$ to be the complement of V_j in V_{j+1}, where $V_{j+1} = V_j + W_j$.

Wavelet multiresolution analysis of $L_2(S)$

Definition

MRA is characterized by the following axioms

- $V^j \subset V^{j+1}$ (subspaces are nested).
- $\overline{\bigcup_{j=-\infty}^{j=\infty} V_j} = L_2(S)$.
- Each V^j has a Riesz basis of scaling function $\{\phi_k^j | k \in \mathcal{K}^j\}$.

Define $W_j = \{\psi_k^j(\textit{wavelets}) | k \in \mathcal{M}^j\}$ to be the complement of V_j in V_{j+1}, where $V_{j+1} = V_j + W_j$.

Wavelet multiresolution analysis of $L_2(S)$

Definition

MRA is characterized by the following axioms

- $V^j \subset V^{j+1}$ (subspaces are nested).
- $\overline{\bigcup_{j=-\infty}^{j=\infty} V_j} = L_2(S)$.
- Each V^j has a Riesz basis of scaling function $\{\phi_k^j | k \in \mathcal{K}^j\}$.

Define $W_j = \{\psi_k^j (\textit{wavelets}) | k \in \mathcal{M}^j\}$ to be the complement of V_j in V_{j+1}, where $V_{j+1} = V_j + W_j$.

Wavelet multiresolution analysis of $L_2(S)$

Definition

MRA is characterized by the following axioms

- $V^j \subset V^{j+1}$ (subspaces are nested).
- $\overline{\bigcup_{j=-\infty}^{j=\infty} V_j} = L_2(S)$.
- Each V^j has a Riesz basis of scaling function $\{\phi_k^j | k \in \mathcal{K}^j\}$.

Define $W_j = \{\psi_k^j (\textit{wavelets}) | k \in \mathcal{M}^j\}$ to be the complement of V_j in V_{j+1}, where $V_{j+1} = V_j + W_j$.

Construction of spherical wavelets based on spherical triangular grids

The set of all vertices $\mathcal{S}^j = \{p_k^j \in S : p_k^j = p_{2k}^{j+1} | k \in \mathcal{K}^j\}$ and $\mathcal{M}^j = \mathcal{K}^{j+1}/\mathcal{K}^j$.

Level 0

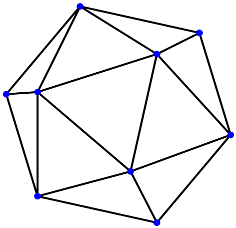

Construction of spherical wavelets based on spherical triangular grids

The set of all vertices $\mathcal{S}^j = \{p_k^j \in S : p_k^j = p_{2k}^{j+1} | k \in \mathcal{K}^j\}$ and $\mathcal{M}^j = \mathcal{K}^{j+1}/\mathcal{K}^j$.

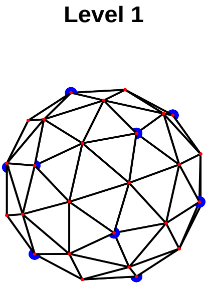

Fast wavelet transform

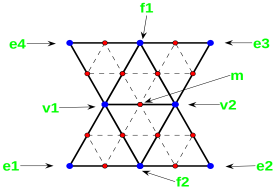

The members of the neighborhoods used in wavelet bases ($m \in \mathcal{M}^j$, $\mathcal{K}_m = \{v_1, v_2, f_1, f_2, e_1, e_2, e_3, e_4\}$).

Analysis(j) :

$$\forall m \in \mathcal{M}^j : d_m^j = c_m^{j+1} - \sum_{k \in \mathcal{K}_m} \tilde{s}_{k,m}^j c_k^j,$$

$$\forall m \in \mathcal{K}^j : c_k^j = c_k^{j+1}.$$

Synthesis(j) :

$$\forall m \in \mathcal{K}^j : c_k^j = c_k^j,$$

$$\forall m \in \mathcal{M}^j : c_m^{j+1} = d_m^j + \sum_{k \in \mathcal{K}_m} \tilde{s}_{k,m}^j c_k^j$$

Fast wavelet transform

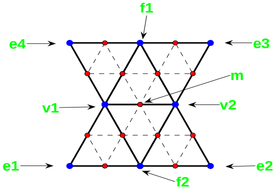

Analysis(j) :

$$\forall m \in \mathcal{M}^j : d_m^j = c_m^{j+1} - \sum_{k \in \mathcal{K}_m} \tilde{s}_{k,m}^j c_k^j,$$

$$\forall m \in \mathcal{K}^j : c_k^j = c_k^{j+1}.$$

Synthesis(j) :

$$\forall m \in \mathcal{K}^j : c_k^j = c_k^j,$$

$$\forall m \in \mathcal{M}^j : c_m^{j+1} = d_m^j + \sum_{k \in \mathcal{K}_m} \tilde{s}_{k,m}^j c_k^j$$

The members of the neighborhoods used in wavelet bases ($m \in \mathcal{M}^j$, $\mathcal{K}_m = \{v_1, v_2, f_1, f_2, e_1, e_2, e_3, e_4\}$).

For linear basis, $\tilde{s}_{v_1} = \tilde{s}_{v_2} = 1/2$

Fast wavelet transform

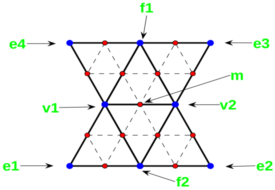

Analysis(j) :

$$\forall m \in \mathcal{M}^j : d_m^j = c_m^{j+1} - \sum_{k \in \mathcal{K}_m} \tilde{s}_{k,m}^j c_k^j,$$

$$\forall m \in \mathcal{K}^j : c_k^j = c_k^{j+1}.$$

Synthesis(j) :

$$\forall m \in \mathcal{K}^j : c_k^j = c_k^j,$$

$$\forall m \in \mathcal{M}^j : c_m^{j+1} = d_m^j + \sum_{k \in \mathcal{K}_m} \tilde{s}_{k,m}^j c_k^j$$

The members of the neighborhoods used in wavelet bases ($m \in \mathcal{M}^j$, $\mathcal{K}_m = \{v_1, v_2, f_1, f_2, e_1, e_2, e_3, e_4\}$).

For Butterfly basis, $\tilde{s}_{v_1} = \tilde{s}_{v_2} = 1/2$, $\tilde{s}_{f_1} = \tilde{s}_{f_2} = 1/8$, $\tilde{s}_{e_1} = \tilde{s}_{e_2} = \tilde{s}_{e_3} = -1/16$

Fast wavelet transform

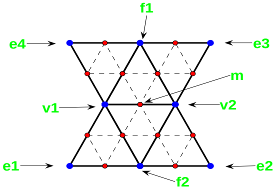

The members of the neighborhoods used in wavelet bases ($m \in \mathcal{M}^j$, $\mathcal{K}_m = \{v_1, v_2, f_1, f_2, e_1, e_2, e_3, e_4\}$).

Analysis(j) :

$$\forall m \in \mathcal{M}^j : d_m^j = c_m^{j+1} - \sum_{k \in \mathcal{K}_m} \tilde{s}_{k,m}^j c_k^j,$$

$$\forall m \in \mathcal{M}^j : c_k^j = c_k^{j+1} + s_{k,m}^j d_m^j.$$

Synthesis(j) :

$$\forall m \in \mathcal{M}^j : c_k^j = c_k^j - \sum_{k \in \mathcal{K}_m} s_{k,m}^j d_m^j,$$

$$\forall m \in \mathcal{M}^j : c_m^{j+1} = d_m^j + \sum_{k \in \mathcal{K}_m} \tilde{s}_{k,m}^j c_k^j$$

Wavelet compression

$$u^J(p) = \sum_{k\in\mathcal{K}^0} c_k^{J_0}\phi_k^{J_0}(p) + \sum_{j=J_0}^{j=J-1}\sum_{m\in\mathcal{M}^j} d_m^j\psi_m^j(p)$$

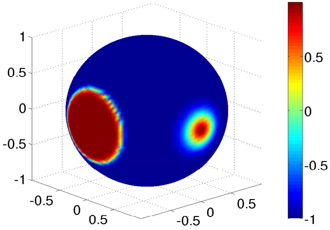

Test function

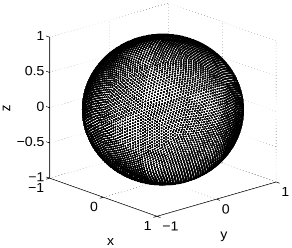

Wavelet locations x_k^J without compression at $J = 5$, $\#\mathcal{K}^5 = 10242$

Wavelet compression

$$u^J_{\geq}(p) = \sum_{k\in\mathcal{K}^0} c^{J_0}_k \phi^{J_0}_k(p) + \sum_{j=J_0}^{j=J-1} \sum_{\substack{m\in\mathcal{M}^j \\ |d^j_m|\geq\epsilon}} d^j_m \psi^j_m(p)$$

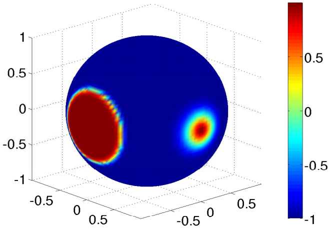

Test function

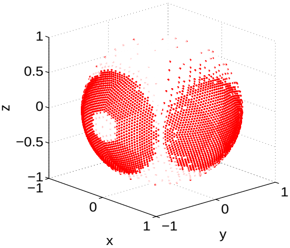

Wavelet locations x^J_k at $J = 5$, $\epsilon = 10^{-5}$, $N(\epsilon) = 995$ and ratio $\frac{\#\mathcal{K}^5}{N(\epsilon)} \approx 10$

Wavelet compression

$$u^J_{\geq}(p) = \sum_{k\in\mathcal{K}^0} c_k^{J_0}\phi_k^{J_0}(p) + \sum_{j=J_0}^{j=J-1} \sum_{\substack{m\in\mathcal{M}^j \\ |d_m^j|\geq\epsilon}} d_m^j \psi_m^j(p)$$

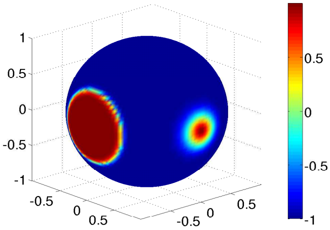

Test function

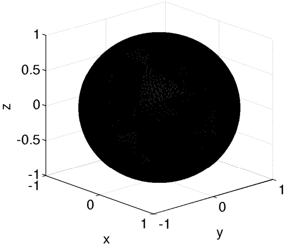

Wavelet locations x_k^J without compression at $J = 6$, $\#\mathcal{K}^6 = 40962$

Wavelet compression

$$u^J_{\geq}(p) = \sum_{k\in\mathcal{K}^0} c^{J_0}_k \phi^{J_0}_k(p) + \sum_{j=J_0}^{j=J-1} \sum_{\substack{m\in\mathcal{M}^j\\ |d^j_m|\geq\epsilon}} d^j_m \psi^j_m(p)$$

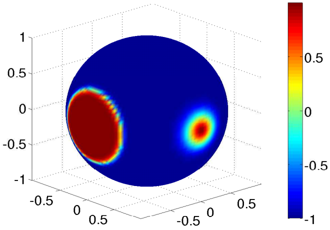

Test function

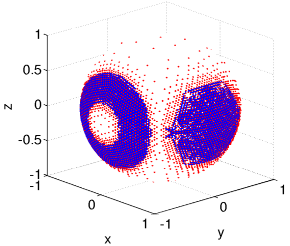

Wavelet locations x^J_k st $J = 6$, $\epsilon = 10^{-5}$, $N(\epsilon) = 8175$ and ratio $\frac{\#\mathcal{K}^6}{N(\epsilon)} \approx 5$

Wavelet compression

$$u_{\geq}^{J}(p) = \sum_{k\in\mathcal{K}^0} c_k^{J_0}\phi_k^{J_0}(p) + \sum_{j=J_0}^{j=J-1} \sum_{\substack{m\in\mathcal{M}^j \\ |d_m^j|\geq\epsilon}} d_m^j\psi_m^j(p)$$

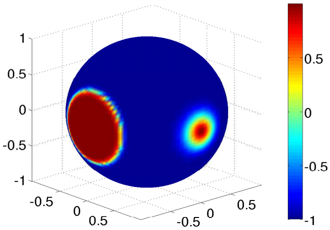

Test function

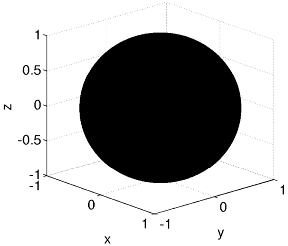

Wavelet locations x_k^J without compression at $J = 7$, $\#\mathcal{K}^7 = 163842$

Wavelet compression

$$u_{\geq}^{J}(p) = \sum_{k\in\mathcal{K}^0} c_k^{J_0}\phi_k^{J_0}(p) + \sum_{j=J_0}^{j=J-1} \sum_{\substack{m\in\mathcal{M}^j \\ |d_m^j|\geq\epsilon}} d_m^j \psi_m^j(p)$$

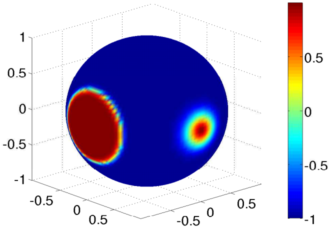

Test function

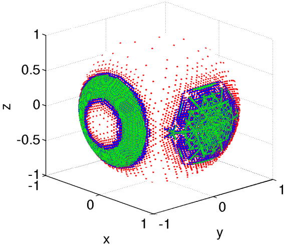

Wavelet locations x_k^J at $J = 7$, $\epsilon = 10^{-5}$, $N(\epsilon) = 20353$ and ratio $\frac{\#\mathcal{K}^7}{N(\epsilon)} \approx 8$

Wavelet compression

$$u^J_{\geq}(p) = \sum_{k\in\mathcal{K}^0} c^{J_0}_k \phi^{J_0}_k(p) + \sum_{j=J_0}^{j=J-1} \sum_{\substack{m\in\mathcal{M}^j \\ |d^j_m|\geq\epsilon}} d^j_m \psi^j_m(p)$$

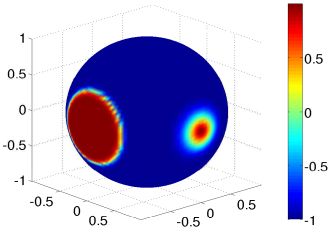

Test function

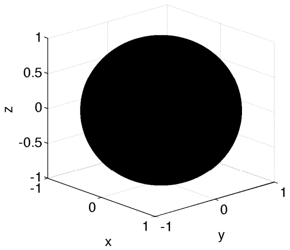

Wavelet locations x^J_k without compression at $J = 8$, $\#\mathcal{K}^8 = 655362$

Wavelet compression

$$u^J_{\geq}(p) = \sum_{k\in\mathcal{K}^0} c_k^{J_0}\phi_k^{J_0}(p) + \sum_{j=J_0}^{j=J-1}\sum_{\substack{m\in\mathcal{M}^j \\ |d^j_m|\geq\epsilon}} d^j_m\psi^j_m(p)$$

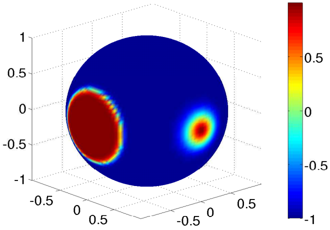

Test function

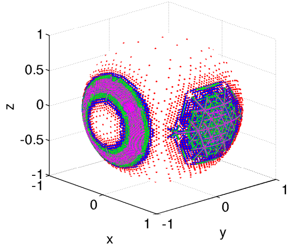

Wavelet locations x_k^J at $J = 8$, $\epsilon = 10^{-5}$, $N(\epsilon) = 64231$ and ratio $\frac{\#\mathcal{K}^8}{N(\epsilon)} \approx 10$

Wavelet approximation estimates

- Approximation error is controlled by the wavelet threshold ϵ
  $||u^J(p) - u^J_{\geq}(p)||_\infty \leq c_1 \epsilon$

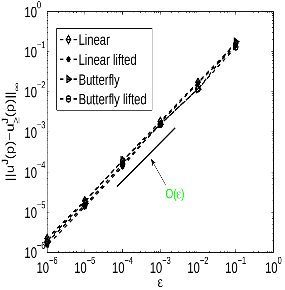

Wavelet approximation estimates

- ϵ controls the total active grid points $N(\epsilon)$ by the following relation $N(\epsilon) \leq c_2 \epsilon^{-\frac{n}{k}}$
- Therefore, approximation error is controlled by active grid points $||u^J(p) - u^J_{\geq}(p)||_\infty \leq c_3 N(\epsilon)^{-\frac{k}{n}}$

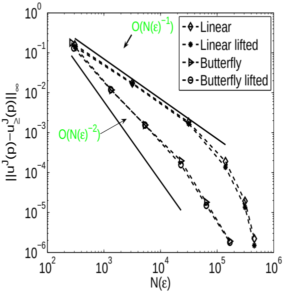

Calculation of Laplace-Beltrami operator on adaptive grid

$$\Delta_{\mathcal{S}} u(p_i^j) = \frac{1}{A_{\mathcal{S}}(p_i^j)} \sum_{k \in N(i)} \frac{\cot \alpha_{i,k} + \cot \beta_{i,k}}{2} [u(p_k^j) - u(p_i^j)]$$

where $A_{\mathcal{S}}(p_i^j)$ is the area of one-ring neighborhood region given by $A_{\mathcal{S}}(p_i^j) = \frac{1}{8} \sum_{k \in N(i)} (\cot \alpha_{i,k} + \cot \beta_{i,k}) \| p_k^j - p_i^j \|^2$.

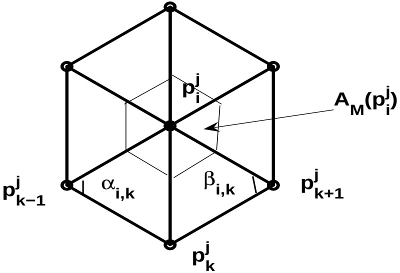

Calculation of Laplace-Beltrami operator on adaptive grid

$$\Delta_{\mathcal{S}} u(p_i^j) = \frac{1}{A_{\mathcal{S}}(p_i^j)} \sum_{k \in N(i)} \frac{\cot \alpha_{i,k} + \cot \beta_{i,k}}{2} [u(p_k^j) - u(p_i^j)]$$

- Convergence result for the Laplace-Beltrami operator of $u_{\geq}^J(p)$ for the test function

$$||\Delta_S u^J(p) - \Delta_S u_{\geq}^J(p)||_\infty \leq c_4 \epsilon$$

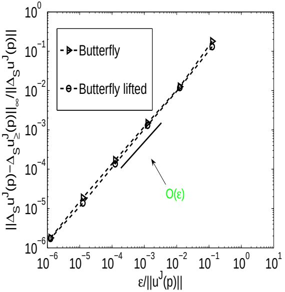

Calculation of Laplace-Beltrami operator on adaptive grid

$$\Delta_{\mathcal{S}} u(p_i^j) = \frac{1}{A_{\mathcal{S}}(p_i^j)} \sum_{k \in N(i)} \frac{\cot \alpha_{i,k} + \cot \beta_{i,k}}{2} [u(p_k^j) - u(p_i^j)]$$

- Convergence result for the Laplace-Beltrami operator of $u^J_{\geq}(p)$ for the test function

$$||\Delta_S u^J(p) - \Delta_S u^J_{\geq}(p)||_\infty \leq c_4 \epsilon \leq c_5 N(\epsilon)^{-\frac{k-2}{n}}$$

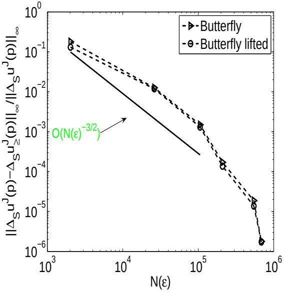

Calculation of other differential operators on adaptive grid

- The flux term present in the spherical advection equation can be expressed in the form of flux divergence and Jacobian operators, $\nabla.(Vu) = \nabla.(u\nabla\chi) - J(u, \psi)$
- $J_S(u(p_i^j), \psi(p_i^j)) = \frac{1}{6A_S(p_i^j)} \sum_{k\in N(i)} (u(p_k^j) + u(p_i^j))(\psi(p_k^j) - \psi(p_i^j))$
- $$\nabla_S.(u(p_i^j), \nabla_S \chi(p_i^j)) = \frac{1}{2A_S(p_i^j)} \sum_{k\in N(i)} \frac{\cot\alpha_{i,k} + \cot\beta_{i,k}}{2} (u(p_k^j) + u(p_i^j))(\psi(p_k^j) - \psi(p_i^j)).$$

Calculation of other differential operators on adaptive grid

- The flux term present in the spherical advection equation can be expressed in the form of flux divergence and Jacobian operators, $\nabla.(Vu) = \nabla.(u\nabla\chi) - J(u,\psi)$
- $J_{\mathcal{S}}(u(p_i^j),\psi(p_i^j)) = \frac{1}{6A_{\mathcal{S}}(p_i^j)}\sum_{k\in N(i)}(u(p_k^j)+u(p_i^j))(\psi(p_k^j)-\psi(p_i^j))$
- $$\nabla_{\mathcal{S}}.(u(p_i^j),\nabla_{\mathcal{S}}\chi(p_i^j)) = \frac{1}{2A_{\mathcal{S}}(p_i^j)}\sum_{k\in N(i)}\frac{\cot\alpha_{i,k}+\cot\beta_{i,k}}{2}(u(p_k^j)+u(p_i^j))(\psi(p_k^j)-\psi(p_i^j)).$$

Calculation of other differential operators on adaptive grid

- The flux term present in the spherical advection equation can be expressed in the form of flux divergence and Jacobian operators, $\nabla.(Vu) = \nabla.(u\nabla\chi) - J(u,\psi)$
- $J_{\mathcal{S}}(u(p_i^j),\psi(p_i^j)) = \frac{1}{6A_{\mathcal{S}}(p_i^j)}\sum_{k\in N(i)}(u(p_k^j)+u(p_i^j))(\psi(p_k^j)-\psi(p_i^j))$
-

$$\nabla_{\mathcal{S}}.(u(p_i^j),\nabla_{\mathcal{S}}\chi(p_i^j)) = \frac{1}{2A_{\mathcal{S}}(p_i^j)}\sum_{k\in N(i)}\frac{\cot\alpha_{i,k}+\cot\beta_{i,k}}{2}(u(p_k^j)+u(p_i^j))(\psi(p_k^j)-\psi(p_i^j)).$$

Calculation of other differential operators on adaptive grid

- The flux term present in the spherical advection equation can be expressed in the form of flux divergence and Jacobian operators, $\nabla.(Vu) = \nabla.(u\nabla\chi) - J(u,\psi)$
- $J_{\mathcal{S}}(u(p_i^j),\psi(p_i^j)) = \frac{1}{6A_{\mathcal{S}}(p_i^j)}\sum_{k\in N(i)}(u(p_k^j)+u(p_i^j))(\psi(p_k^j)-\psi(p_i^j))$
- $$\nabla_{\mathcal{S}}.(u(p_i^j),\nabla_{\mathcal{S}}\chi(p_i^j)) = \frac{1}{2A_{\mathcal{S}}(p_i^j)}\sum_{k\in N(i)}\frac{\cot\alpha_{i,k}+\cot\beta_{i,k}}{2}(u(p_k^j)+u(p_i^j))(\psi(p_k^j)-\psi(p_i^j)).$$

Application of spherical wavelets to compress turbulence

- Turbulence can be divided into two orthogonal parts: a organized (coherent vortices), inhomogeneous, non-Gaussian component and random noise (incoherent), homogeneous and Gaussian component.
- The coherent vortices must be resolved, but the noise may be modeled (or neglected entirely).
- The coherent vortices can be extracted using nonlinear wavelet filtering.

This is the concept of Coherent Vortex Simulation which was developed by Marie Farge, Kai Schneider and Nicholas Kevlahan in flat geometries.

Application of spherical wavelets to compress turbulence

- Turbulence can be divided into two orthogonal parts: a organized (coherent vortices), inhomogeneous, non-Gaussian component and random noise (incoherent), homogeneous and Gaussian component.
- The coherent vortices must be resolved, but the noise may be modeled (or neglected entirely).
- The coherent vortices can be extracted using nonlinear wavelet filtering.

This is the concept of Coherent Vortex Simulation which was developed by Marie Farge, Kai Schneider and Nicholas Kevlahan in flat geometries.

Application of spherical wavelets to compress turbulence

- Turbulence can be divided into two orthogonal parts: a organized (coherent vortices), inhomogeneous, non-Gaussian component and random noise (incoherent), homogeneous and Gaussian component.
- The coherent vortices must be resolved, but the noise may be modeled (or neglected entirely).
- The coherent vortices can be extracted using nonlinear wavelet filtering.

This is the concept of Coherent Vortex Simulation which was developed by Marie Farge, Kai Schneider and Nicholas Kevlahan in flat geometries.

Application of spherical wavelets to compress turbulence

- Turbulence can be divided into two orthogonal parts: a organized (coherent vortices), inhomogeneous, non-Gaussian component and random noise (incoherent), homogeneous and Gaussian component.
- The coherent vortices must be resolved, but the noise may be modeled (or neglected entirely).
- The coherent vortices can be extracted using nonlinear wavelet filtering.

This is the concept of Coherent Vortex Simulation which was developed by Marie Farge, Kai Schneider and Nicholas Kevlahan in flat geometries.

Application of spherical wavelets to compress turbulence

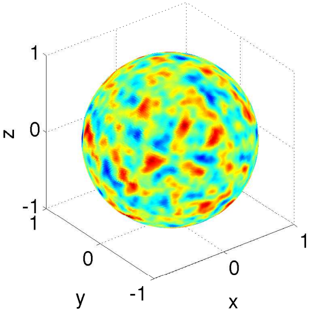

Vorticity function.

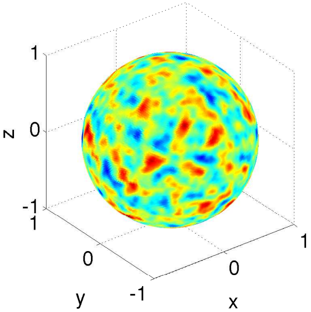

Reconstructed with 40% significant wavelets.

Application of spherical wavelets to compress turbulence

$$E(n,0) = \frac{\mathcal{A} n^{\gamma/2}}{(n+n_0)^{\gamma}}$$

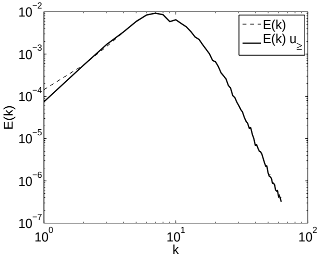

Energy spectrum reconstructed with 40% significant wavelets.

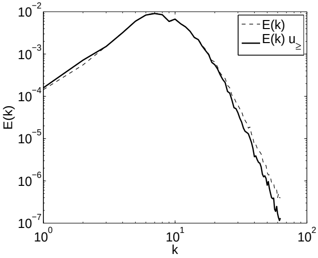

Energy spectrum reconstructed with 2% significant wavelets

Application of spherical wavelets to compress turbulence

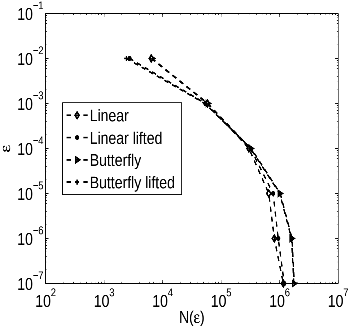

Relation between ϵ and $N(\epsilon)$ for the vorticity function.

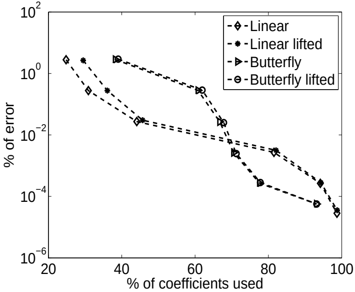

Rate of relative error as a function of rate of significant coefficients $= \frac{N(\epsilon) \times 100}{N(\epsilon=0)}$.

Diffusion equation

$$u_t = \nu \Delta_S u + f$$

where f is localized source chosen such a way that the solution of diffusion equation is given by

$$u(\theta, \phi, t) = 2e^{-\frac{(\theta-\theta_0)^2+(\phi-\phi_0)^2}{\nu(t+1)}}$$

Such equations arise in the application of Willmore flow, surface diffusion flow etc.

Diffusion Equation

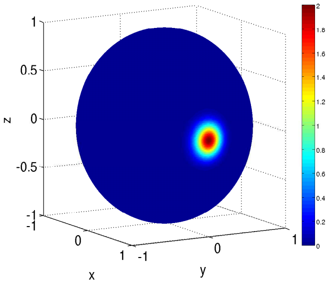

Initial condition at $t = 0$

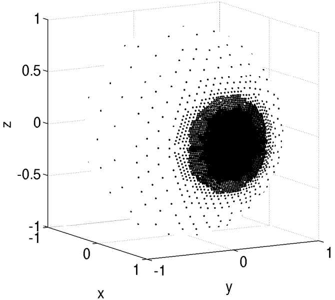

Adaptive grid at $t = 0$

Diffusion Equation

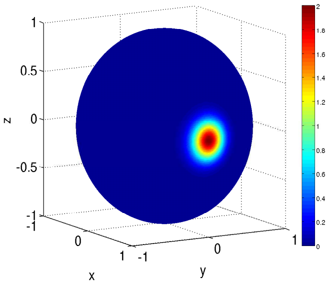

Solution using AWCM at $t = 0.5$

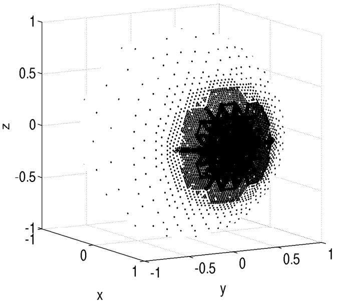

Adaptive grid at $t = 0.5$

Diffusion Equation

The potential of adaptive algorithm is measured by compression coefficients

$$\mathcal{C} = \frac{N(\epsilon = 0)}{N(\epsilon)}$$

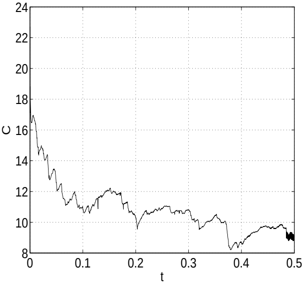

The compression coefficient $\mathcal{C}$ as a function of time, $\epsilon = 10^{-5}$.

Spherical advection equation

$$\frac{\partial u}{\partial t} + V.\nabla_S u = 0,$$

The nondivergent driving velocity field $V = (v_1, v_2)$ for all times is given by

$$v_1 = u_0 \left(\cos(\theta)\cos(\alpha) + \sin(\theta)\cos(\phi + \frac{3\pi}{2})\sin(\alpha) \right),$$

$$v_2 = -u_0 \sin(\phi + \frac{3\pi}{2})\sin(\alpha).$$

Spherical advection equation

$$\frac{\partial u}{\partial t} + V.\nabla_S u = 0,$$

The initial cosine bell test pattern to be advected is given by

$$u(\theta,\phi) = \begin{cases} \frac{u_0}{2}\left(1+\cos(\frac{\pi r}{R}\right) & \text{if } r < R \\ 0 & \text{if } r \geq R, \end{cases}$$

where $u_0 = 1000$m, radius $R = a/3$ and $r = a$ arc $\cos[\sin(\theta_c)\sin(\theta) + \cos(\theta_c)\cos(\theta)\cos(\phi - \phi_c)$, which is the great circle distance between (ϕ,θ) and the center $(\phi_c,\theta_c) = (0,0)$.

Such equations arise typically in the context of numerical weather forecast or in climatological studies, and they provide some of the most challenging and CPU time consuming problems in modern computational fluid dynamics.

Spherical advection equation

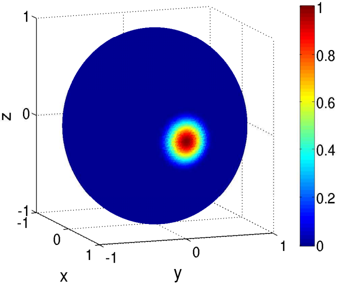

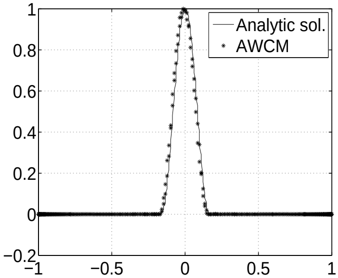

Solid body rotation of cosine bell using AWCM for $\epsilon = 10^{-5}$.

Spherical advection equation

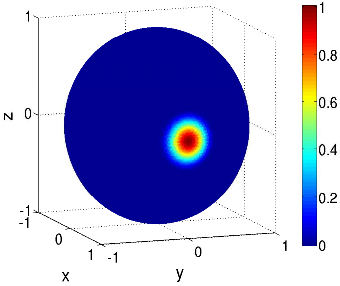

Solution using AWCM

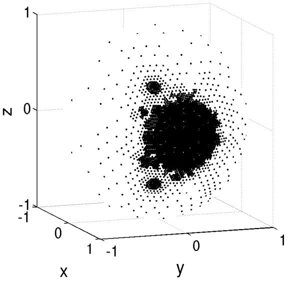

Adapted grid for the solution.

Spherical advection equation

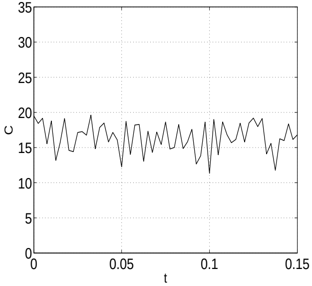

The compression coefficient $\mathcal{C}$ as a function of time, $\epsilon = 10^{-5}$.

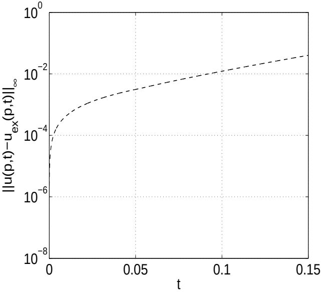

Time evolution of the pointwise L_∞ error of the solution.

Conclusions

Adaptive wavelet collocation method:

- Used for time evolution problems.
- Dynamic adaptivity is necessary for atmospheric modeling.
- Fast $O(\mathcal{N})$ wavelet transform and $O(\mathcal{N})$ hierarchical finite difference schemes over triangulated surface for the differential operators is used.
- Verified convergence result predicted in theory.

Conclusions

Adaptive wavelet collocation method:

- Used for time evolution problems.
- Dynamic adaptivity is necessary for atmospheric modeling.
- Fast $O(\mathcal{N})$ wavelet transform and $O(\mathcal{N})$ hierarchical finite difference schemes over triangulated surface for the differential operators is used.
- Verified convergence result predicted in theory.

Conclusions

Adaptive wavelet collocation method:

- Used for time evolution problems.
- Dynamic adaptivity is necessary for atmospheric modeling.
- Fast $O(\mathcal{N})$ wavelet transform and $O(\mathcal{N})$ hierarchical finite difference schemes over triangulated surface for the differential operators is used.
- Verified convergence result predicted in theory.

Conclusions

Adaptive wavelet collocation method:

- Used for time evolution problems.
- Dynamic adaptivity is necessary for atmospheric modeling.
- Fast $O(\mathcal{N})$ wavelet transform and $O(\mathcal{N})$ hierarchical finite difference schemes over triangulated surface for the differential operators is used.
- Verified convergence result predicted in theory.

Conclusions

Adaptive wavelet collocation method:

- Used for time evolution problems.
- Dynamic adaptivity is necessary for atmospheric modeling.
- Fast $O(\mathcal{N})$ wavelet transform and $O(\mathcal{N})$ hierarchical finite difference schemes over triangulated surface for the differential operators is used.
- Verified convergence result predicted in theory.

Future directions

- Implementation of wavelet bases based on optimal spherical triangulation.

Ref.:Discrete Laplace-Beltrami operator on sphere and optimal spherical triangulation, Int. J. Comp. Geometry Appl. 16 (1) (2006) 75-93.

- Incorporation of appropriate time integration method in spherical domain which takes advantage of wavelet multilevel decomposition.

Ref.:An adaptive multilevel wavelet collocation method for elliptic problems, J. Comp. Phys. 206 (2005) 412-431.

- Application of AWCM to more realistic models.

Future directions

- Implementation of wavelet bases based on optimal spherical triangulation.

Ref.:Discrete Laplace-Beltrami operator on sphere and optimal spherical triangulation, Int. J. Comp. Geometry Appl. 16 (1) (2006) 75-93.

- Incorporation of appropriate time integration method in spherical domain which takes advantage of wavelet multilevel decomposition.

Ref.:An adaptive multilevel wavelet collocation method for elliptic problems, J. Comp. Phys. 206 (2005) 412-431.

- Application of AWCM to more realistic models.

Future directions

- Implementation of wavelet bases based on optimal spherical triangulation.

Ref.:Discrete Laplace-Beltrami operator on sphere and optimal spherical triangulation, Int. J. Comp. Geometry Appl. 16 (1) (2006) 75-93.

- Incorporation of appropriate time integration method in spherical domain which takes advantage of wavelet multilevel decomposition.

Ref.:An adaptive multilevel wavelet collocation method for elliptic problems, J. Comp. Phys. 206 (2005) 412-431.

- Application of AWCM to more realistic models.

Future directions

- Implementation of wavelet bases based on optimal spherical triangulation.

Ref.:Discrete Laplace-Beltrami operator on sphere and optimal spherical triangulation, Int. J. Comp. Geometry Appl. 16 (1) (2006) 75-93.

- Incorporation of appropriate time integration method in spherical domain which takes advantage of wavelet multilevel decomposition.

Ref.:An adaptive multilevel wavelet collocation method for elliptic problems, J. Comp. Phys. 206 (2005) 412-431.

- Application of AWCM to more realistic models.